### **Article**



# Signaling in microbial communities with open boundaries

James J. Winkle, <sup>1</sup> Soutick Saha, <sup>2</sup> Joseph Essman, <sup>3</sup> Matthew R. Bennett, <sup>3,\*</sup> William Ott, <sup>1,\*</sup> Krešimir Josić, <sup>1,3,4,\*</sup> and Andrew Mugler <sup>2,5,\*</sup>

<sup>1</sup>Department of Mathematics, University of Houston, Houston, Texas; <sup>2</sup>Department of Physics and Astronomy, Purdue University, West Lafayette, Indiana; <sup>3</sup>Department of BioSciences, Rice University, Houston, Texas; <sup>4</sup>Department of Biology and Biochemistry, University of Houston, Houston, Texas; and <sup>5</sup>Department of Physics and Astronomy, University of Pittsburgh, Pennsylvania

ABSTRACT Microbial communities such as swarms or biofilms often form at the interfaces of solid substrates and open fluid flows. At the same time, in laboratory environments these communities are commonly studied using microfluidic devices with media flows and open boundaries. Extracellular signaling within these communities is therefore subject to different constraints than signaling within classic, closed-boundary systems such as developing embryos or tissues, yet is understudied by comparison. Here, we use mathematical modeling to show how advective-diffusive boundary flows and population geometry impact cell-cell signaling in monolayer microbial communities. We reveal conditions where the intercellular signaling lengthscale depends solely on the population geometry and not on diffusion or degradation, as commonly expected. We further demonstrate that diffusive coupling with the boundary flow can produce signal gradients within an isogenic population, even when there is no flow within the population. We use our theory to provide new insights into the signaling mechanisms of published experimental results, and we make several experimentally verifiable predictions. Our research highlights the importance of carefully evaluating boundary dynamics and environmental geometry when modeling microbial cell-cell signaling and informs the study of cell behaviors in both natural and synthetic systems.

SIGNIFICANCE Microbial communities in natural environments and microfluidic devices are often exposed to open boundaries and flows, but models used to characterize diffusive signaling in such systems often ignore how device geometry, boundary conditions, and media flow influence signaling behavior. We demonstrate how the effective signaling capacity of these communities can be shaped by population geometry and advective-diffusive boundary flow in quasi-2D environments. Our approach provides a general framework to understand and control advection-reaction-diffusion systems—and their interactions with cellular signaling networks—in both natural and synthetic environments.

#### INTRODUCTION

Diffusive signaling coordinates multicellular processes from embryogenesis and tissue development (1) to microbial quorum sensing (QS) (2–6). In the classical picture of diffusive signaling, the diffusible components are confined to the vicinity of the cells, either by external barriers such as an embryonic envelope, or by the cell membranes themselves in the case of direct cell-to-cell molecular exchange. In these cases, global signaling properties are determined by

basic transport parameters such as the diffusivity of the signaling molecule or the speed of advective flow within the cell population (7).

However, in other cases, the diffusible components are free to escape at the population boundaries, or are otherwise affected by properties of the surrounding medium such as fluid flow. These cases include microbial communities such as biofilms or swarms, whose boundaries are usually open and dynamic, and which often form at the interfaces of solid substrates and fluid flows (8,9). In such environments, responses at the macroscopic (population) level depend on both the features of the domain in which the cells grow and the dynamics of the constituent cells. In particular, open boundaries can significantly impact signaling behavior within the community. Such impacts include modulation of signaling depth and spatial signaling profiles (10), changes

Submitted January 19, 2023, and accepted for publication June 5, 2023.

\*Correspondence: matthew.bennett@rice.edu or ott@math.uh.edu or kjosic@uh.edu or andrew.mugler@pitt.edu

James J. Winkle and Soutick Saha contributed equally to this work.

Editor: N.G. Cogan.

https://doi.org/10.1016/j.bpj.2023.06.002

© 2023 Biophysical Society.



to QS thresholds (9,11), and new challenges when responding to time-varying flows in a spatiotemporally robust manner (8,12). Despite the importance of these impacts, signaling in open geometries has been understudied relative to signaling in closed geometries. In particular, although the effects of open fluid flow overtop a microbial layer have been studied with modeling and experiments (9,11), the effects of flow around the edges of a layer have not, to our knowledge. When cell populations are very thin (e.g., a monolayer), the effects of overtop flow need only propagate a cell diameter to impact signaling properties, whereas the effects of edge flow would need to propagate a length commensurate with the entire population to do so. As we will show, open geometries can induce counterintuitive signaling characteristics, even when the open boundaries are restricted to the edges.

Laboratory experiments aimed at characterizing signaling in microbial communities often rely on microfluidic devices. Such experiments allow researchers to characterize the behavior of spatially extended systems, thereby facilitating the design of microbial consortia that maintain desired population fractions (13) or produce emergent spatiotemporal patterns (14). Here, signaling provides the necessary intercellular communication pathway to coordinate responses and achieve population-level phenotypes. In typical microfluidic experiments, cells are forced to grow in a monolayer, thereby allowing for imaging of large populations at high resolution. Such imaging capability facilitates the investigation of consortia-scale spatiotemporal dynamics, emergent collective behavior, and nematic effects (15,16). Importantly, many microfluidic devices employ open boundaries between the cell population and the surrounding fluid to supply media to cells and remove waste products and excess cells. Open boundary geometries can strongly impact the dynamics of growing microbial collectives and therefore place such microfluidic devices into the same understudied paradigm as the aforementioned biofilms and swarms.

Here, we use mathematical modeling to investigate the effects of open, advective boundaries on cell-cell signaling within a bacterial monolayer. Surprisingly, in contrast to the closed-boundary case, we find that the spatial extent of signaling from a source cell does not depend on the diffu-

sion coefficient, but rather depends entirely on the population geometry. When the signal can degrade, we find that the signaling extent is determined by the minimum of the geometric lengthscale and the classical lengthscale set by the ratio of diffusion to degradation. Furthermore, we find that flow at the boundary can introduce signal gradients within the population—even if flow is absent within the population itself—due to the diffusive exchange of signaling molecules with the boundary region. We compare our results to published data on bacterial monolayers in a microfluidic device that signal via a QS factor.

#### **RESULTS**

We consider a continuum model of bacteria in a monolayer (Fig. 1 A). Such monolayer configurations are typical of the leading edge of growing colonies or biofilms (17–19) and are often imposed by thin cell-trapping regions in microfluidic devices (4,5,10) (Fig. 1 B). To investigate boundary effects, we confine the monolayer to a rectangle with length L and width w. These parameters can be thought of as the characteristic lengthscales of a natural population, or as the precise dimensions of the rectangular trapping region in a microfluidic device. We specify the boundary conditions in detail in the following sections.

To investigate intercellular signaling, we suppose that cells secrete a molecule at a constant rate  $\alpha$  that can diffuse with coefficient D and degrade with rate  $\gamma$ . Secretion of diffusible molecules is a ubiquitous signaling strategy in bacteria, employed in natural functions such as QS (20,21), and probed or engineered in microfluidic experiments (4,5,11,22). In the following sections, we investigate the effects of open boundaries and fluid flow on the properties of such signaling in steady state.

## Open boundaries and constant signal production make the signaling lengthscale independent of diffusion

We first investigate the spatial extent of signaling from a given source cell, without flow; we consider flow in a

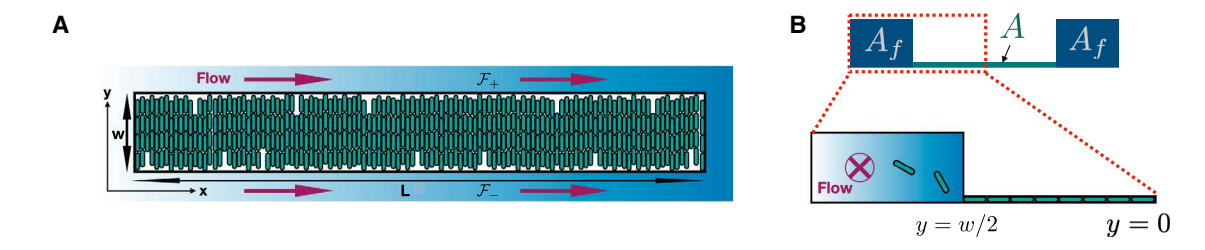


FIGURE 1 We model bacteria growing in a spatially extended microfluidic device using a continuum framework. (A) Top view of the device. Cells are confined to a thin trapping region  $\mathcal{T}$  of width w and length L, wherein they grow in a monolayer. The trapping region interfaces with two three-dimensional flow channels, an upper flow channel  $\mathcal{F}_+$  and a lower flow channel  $\mathcal{F}_-$ . The boundaries between the trapping region and the flow channels are open and therefore subject to flow effects. (B) Side view of the device. The trapping region has cross-sectional area A. Flow channels each have cross-sectional area  $A_f$ . To see this figure in color, go online.

subsequent section. To investigate the spatial extent of signaling, it is often convenient to consider some cells as "senders" of the signaling molecules and other cells as "receivers." For example, in a system with closed boundaries, such as a developing embryo, signaling molecules are "sent" from one end of the embryo and "received" by cell nuclei in the bulk of the embryo (7). Similarly, in microbial communities, often one subpopulation of cells secretes a diffusible signal that a second subpopulation receives, as has been realized and studied in microfluidic experiments (10,23).

In the case of a developing embryo, the classic synthesisdiffusion-clearance model (7) predicts that the signal will establish an exponential concentration profile in steady state. With molecular diffusion coefficient D and degradation rate  $\gamma$ , this profile will have a lengthscale  $\lambda =$  $\sqrt{D/\gamma}$ , given that the system is long  $(L \gg \lambda)$ . The experimental devices we model have length much longer than width  $(L \gg w, \text{ see Fig. 2})$ , such that this assumption establishes a consistent basis for comparison. However, with open boundaries, molecules can leave the system not just by degrading but also by diffusing across the boundary. It is thus unclear what effect open boundaries will have on the signaling lengthscale.

To address this question, we consider the sender-receiver system shown in Fig. 2 A, where cells in the left half of the trapping region T (x < 0) produce the diffusible signal, and cells in the right half ( $x \ge 0$ ) do not. We assume a zero-order functional form for signal production and initially no chemical degradation of the signaling molecules. Our system thus models engineered microbial strains with constitutive or inducible promoters and without signaling feedback. Such systems allow isolation of diffusible-signal communication from the canonical QS mechanism in studies of microbial consortia (10,24). Although we only consider the zero-order functional form for signal production, we examine the impact of first-order degradation (below).

The signal concentration c(x, y) obeys the diffusion equation with production rate  $\alpha$ ,

$$\dot{c} = D\nabla^2 c + \alpha [1 - \theta(x)], \tag{1}$$

where the Heaviside function  $\theta(x)$  ensures that signal production only occurs for x < 0. Here, c has units of molecules per volume (and thus a has units of volumetric concentration per time) even though it only varies in the x- and y-directions. Because we are interested in open boundaries, where molecules can be lost by diffusion, degradation is not required for c to reach steady state. Signaling molecules often have a large half-life, and are not absorbed into microfluidic device material (25). Therefore, we neglect degradation here, and we consider its effects in the next section.

Eq. 1 does not capture diffusion of signaling molecules through the cell membrane, but rather describes the dynamics of signaling molecule concentration in extracellular space. A more detailed model would include separate partial

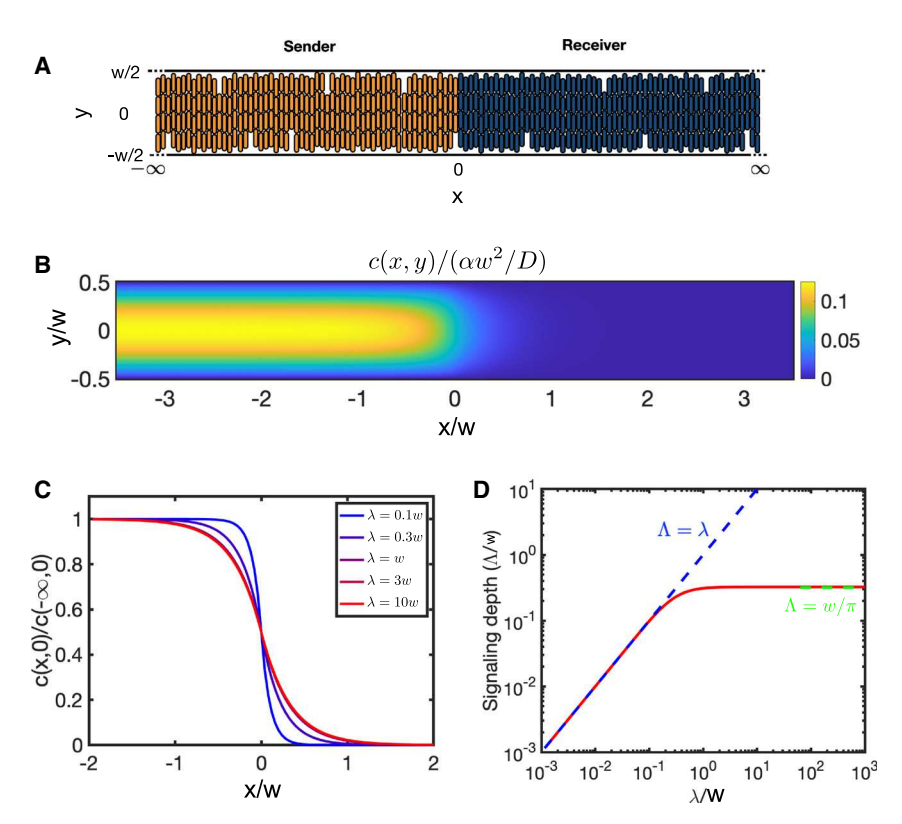


FIGURE 2 Signaling lengthscale in a "senderreceiver" setup. (A) Cells on the left (orange) secrete a diffusible signal, whereas cells on the right (blue) do not. (B) Steady-state concentration profile with no signal degradation (Eq. 5). (C) Signal profile at the midline (y = 0) with degradation rate  $\gamma$ (Eq. 9), characterized by diffusion lengthscale  $\lambda =$  $\sqrt{D/\gamma}$ . (D) With degradation, signaling is limited by the minimum of  $\lambda$  and  $kw/\pi$ , where w is the lengthscale of the trapping region, see (A) and  $k \approx 1$ . To see this figure in color, go online.

differential equation (PDEs) for intracellular and extracellular compartments coupled via diffusion through the cell membrane. However, here we capture the combined effects of molecule production and secretion into the extracellular space with a single rate,  $\alpha$ . Eq. 1 then describes diffusion of signaling molecules within the extracellular space.

Eq. 1 also neglects cell growth. We are interested in the diffusion of molecules over distances w on the order of 100  $\mu$ m, with diffusion coefficient D on the order of hundreds of microns squared per second. We therefore neglect cell growth because the typical diffusion timescale  $w^2/D$ is tens of seconds, which is much smaller than the typical growth and division timescale of tens of minutes to hours.

To determine the effect of open boundaries, we assume that the upper and lower boundaries  $(y = \pm w/2)$  between the trapping region and the flow channels are absorbing with respect to the signaling molecule, so that the signal concentration vanishes there:

$$c(x, \pm w/2) = 0.$$
 (2)

We will see later that absorbing boundary conditions are appropriate if we assume the flow speed is large, an assumption we make for our sender-receiver analysis. Since we are modeling a long system  $(L \gg w)$ , we take  $L \to \infty$ . A senderreceiver system of precisely this type (with open boundaries at  $y = \pm w/2$  and with  $L \gg w$ ) was created in microfluidic experiments in previous work (10). We compare our predictions to these experiments in the discussion.

Far from the sender cells, the signal concentration must vanish:

$$c(\infty, y) = 0. (3)$$

(5)

Far from the receiver cells, the concentration must become independent of x. The diffusion equation there reads  $\dot{c} = D\partial_{\nu}^2 c + \alpha$ , which in steady state and with Eq. 2 is solved by

$$c(-\infty, y) = \frac{\alpha w^2}{D} f(y), \text{ with } f(y) = \frac{1}{8} - \frac{y^2}{2w^2}.$$
 (4)

With the four boundary conditions in Eqs. 2, 3, and 4, we solve Eq. 1 in steady state by separating variables and ensuring continuity of the solution and its derivative at the sender-receiver interface (appendix A). The result is

$$c(x,y) = \frac{\alpha w^2}{D} \begin{cases} f(y) - \sum_{n=0}^{\infty} a_n e^{q_n x/w} \cos(q_n y/w) & x < 0 \\ \sum_{n=0}^{\infty} a_n e^{-q_n x/w} \cos(q_n y/w) & x \ge 0, \end{cases}$$

where  $a_n \equiv 2(-1)^n/q_n^3$  and  $q_n \equiv \pi(2n+1)$ . The signal concentration given by Eq. 5 is shown in Fig. 2 B. The concentration vanishes at the open boundaries and decays across the sender-receiver interface.

The signaling lengthscale is set by the decay length of the concentration profile in the right half ( $x \ge 0$ ) of the trapping region. The decay length is obtained by integrating the profile, normalized by its value at the interface (x = 0). Doing so along the midline (y = 0), we obtain a measure of signaling depth,

$$\Lambda = \int_0^\infty dx \frac{c(x,0)}{c(0,0)} = \frac{kw}{\pi},\tag{6}$$

where  $k \equiv \pi(\sum_{n=0}^{\infty} a_n/q_n)/\sum_{n'=0}^{\infty} a_{n'} \approx 1.021$ . We observe that, since the coefficients  $a_n$  fall off rapidly as  $n^{-3}$ , Eq. 6 is well approximated by the fundamental of the series solution and the resulting approximate signaling depth is  $w/\pi$  to first order.

Eq. 6 shows that the signaling lengthscale  $\Lambda$  depends only on w, the width of the trapping region between the two open boundaries. Surprisingly, it is independent of the diffusion coefficient, D. In fact, the lack of a diffusion-dependent lengthscale is already apparent in Eq. 5, where we see that D factors out of the solution and is absent from the exponential x dependence. Thus the diffusion coefficient affects the overall amplitude of the signal, but not how it decays with distance from the sender-receiver interface.

The mathematical reason that Eq. 6 does not depend on D is that Eq. 1 involves only a zero-order reaction (26,27), namely production at the constant rate  $\alpha$ . Consequently, all parameters in Eq. 1 can be removed by scaling length by w, time by  $w^2/D$ , and concentration by  $\alpha w^2/D$ . All lengthscales must then depend only on w, as demonstrated in Eqs. 5 and 6. We will see in the next section that this restriction no longer holds when adding the first-order degradation reaction.

The physical reason that Eq. 6 does not depend on D is the following. When diffusion increases, the amplitude of the profile decreases, in both open and closed systems, as diffusion spreads the signaling molecules across space. In closed systems, this spreading leads to an increased signaling lengthscale as higher diffusion allows molecules to travel farther from the source. However, in open systems, increasing the spread of molecules across space also increases the rate at which they cross the open boundaries. Molecules that would have diffused farther from the source if boundaries were closed are the ones that are more likely to be lost. In systems with open boundaries, the two opposing effects of signal loss across the open boundaries and signal diffusion cancel exactly, so that the signaling lengthscale is independent of diffusion.

#### With degradation, the signaling lengthscale is bounded from above by the geometry

Degrading enzymes can introduce active degradation in microbial populations. For example, expression of AiiA lactonase can significantly accelerate the degradation of signaling molecules inside bacteria (28), which can translate to an effective extracellular molecule loss for sufficiently

fast diffusion across the membrane. Moreover, extracellular signal degradation can be induced and controlled in engineered microbial consortia (6,29).

To examine how degradation impacts signaling in open geometries and to more directly compare the behavior of our model with that of the closed-boundary synthesis-diffusion-clearance model, we introduce degradation with rate  $\gamma$  into Eq. 1:

$$\dot{c} = D\nabla^2 c + \alpha [1 - \theta(x)] - \gamma c. \tag{7}$$

The solution far from the receiver cells generalizes from Eq. 4 to

$$c(-\infty, y) = \frac{\alpha w^2}{D} F(y), F(y) = \frac{\lambda^2}{w^2} \left[ 1 - \frac{\cosh(y/\lambda)}{\cosh(w/2\lambda)} \right],$$
(8)

where  $\lambda = \sqrt{D/\gamma}$  is the closed-boundary diffusion lengthscale. We use  $c(-\infty, y)$  as a boundary condition for Eq. 7 together with the boundary conditions given in Eqs. 2 and 3. Solving Eq. 7 using the same approach as in the previous section (appendix A), we obtain

$$c(x,y) = \frac{\alpha w^2}{D} \begin{cases} F(y) - \sum_{n=0}^{\infty} A_n e^{x/\ell_n} \cos(q_n y/w) & x < 0 \\ \sum_{n=0}^{\infty} A_n e^{-x/\ell_n} \cos(q_n y/w) & x \ge 0, \end{cases}$$

where  $A_n = 2(-1)^n (\ell_n/w)^2/q_n$  and  $\ell_n = w\lambda/\sqrt{q_n^2\lambda^2 + w^2}$ . Note that, in the zero-degradation limit  $(\lambda \gg w)$ , we have  $F(y) \rightarrow f(y)$ ,  $\ell_n \rightarrow w/q_n$ ,  $A_n \rightarrow a_n$ , and Eq. 9 reduces to Eq. 5, as expected.

The solution given by Eq. 9 is shown in Fig. 2 C, where we see that the signal penetrates more deeply into the receiver cell population as  $\lambda$  increases, but that the signaling depth eventually saturates. Indeed, with degradation the penetration depth of the signal defined in Eq. 6 becomes

$$\Lambda = \frac{\sum_{n=0}^{\infty} A_n \ell_n}{\sum_{n'=0}^{\infty} A_{n'}} \to \begin{cases} kw/\pi & \lambda \gg w \\ \lambda & \lambda \ll w, \end{cases}$$
(10)

where the second case follows from the fact that  $\ell_n \to \lambda$  for  $\lambda \ll w$ . Eq. 10 is plotted in Fig. 2 D. We recover the diffusion-independent result given by Eq. 6 in the limit of small degradation,  $\lambda \gg w$ . In this limit, signal loss due to diffusion into the flow channels dominates over signal loss due to degradation. When degradation is strong,  $\lambda \ll w$ , signaling depth approaches the closed-boundary length-scale,  $\lambda$ . In this limit, signaling molecules typically degrade before they diffuse into the flow channels. Overall, we have

$$\Lambda \le \min\{\lambda, kw / \pi\},\tag{11}$$

a bound that reflects the influence of both degradation and open boundaries on signaling depth.

### Flow outside the population introduces signal gradients within the population

Thus far we have considered the effects of open boundaries, but not fluid flow in the boundary regions. Surrounding flows are common in natural settings (8,12), and flow is often desired or operationally necessary in channels bounding the trapping region in a microfluidic device (30,31). To investigate the effects of boundary flow on signaling in a bacterial population, we return to the simplest case of a homogeneous population (all cells secrete the signal) with no signal degradation (Fig. 3 A). We introduce flow at a constant velocity v in the x-direction within the flow channels  $\mathcal{F}_{\pm}$  that lie outside the upper and lower boundaries of the trapping region ( $y = \pm w/2$ ). Because flow breaks the translational symmetry of the signal profile in the x-direction, we assume the length of the trapping region, L, is finite.

We assume that the signaling molecule concentration in the flow channels does not depend on the *z*-direction. Indeed, this type of dimension reduction is often performed when studying pollutant transport in rivers (32) or shallowwater flows (33). Below we eliminate dependence on the *y*-direction as well, and we justify the overall reduction by comparing a mixing timescale within cross sections of the flow channels with an advective lengthscale. See (8) for a similar approach to dimension reduction.

Let  $b_{\pm}(x,y)$  denote the volumetric concentration of signaling molecule in  $\mathcal{F}_{\pm}$ . The dynamics in the trapping region and flow channels obey

$$\dot{c} = D\nabla^2 c + \alpha,\tag{12}$$

$$\dot{b}_{+} = D\nabla^{2}b_{+} - v\partial_{x}b_{+}, \qquad (13)$$

where  $\alpha$  is the signal production rate and  $\nu$  is the flow velocity. Although cells can exit the trapping region and enter the flow channels, we assume that signal production in the channels is negligible. We also assume that there is no flow in the trapping region. However, the trapping region and the flow channels are coupled by diffusion of molecules across the boundaries. Correspondingly, we impose continuity of the profiles at the boundaries,

$$c(x, \pm w/2) = b_{+}(x, \pm w/2),$$
 (14)

as well as their derivatives,  $\partial_y c|_{y=\pm w/2} = \partial_y b_{\pm}|_{y=\pm w/2}$ .

To solve Eqs. 12 and 13 in steady state, we assume that, whereas the concentration in the flow channels changes in the x-direction due to the flow, it is constant in the y-direction, so that  $b_+(x,y) = b_-(x,y) = b(x)$ . Such an approximation is valid when the length L of the flow channels is an order of magnitude larger than their width (32). This length-to-width ratio is on the order of 200 : 1 for the experimental devices we model. Justifying our assumption that signaling molecule concentration depends only on x more carefully, we argue that signaling molecule concentration quickly homogenizes in each cross section of each flow channel

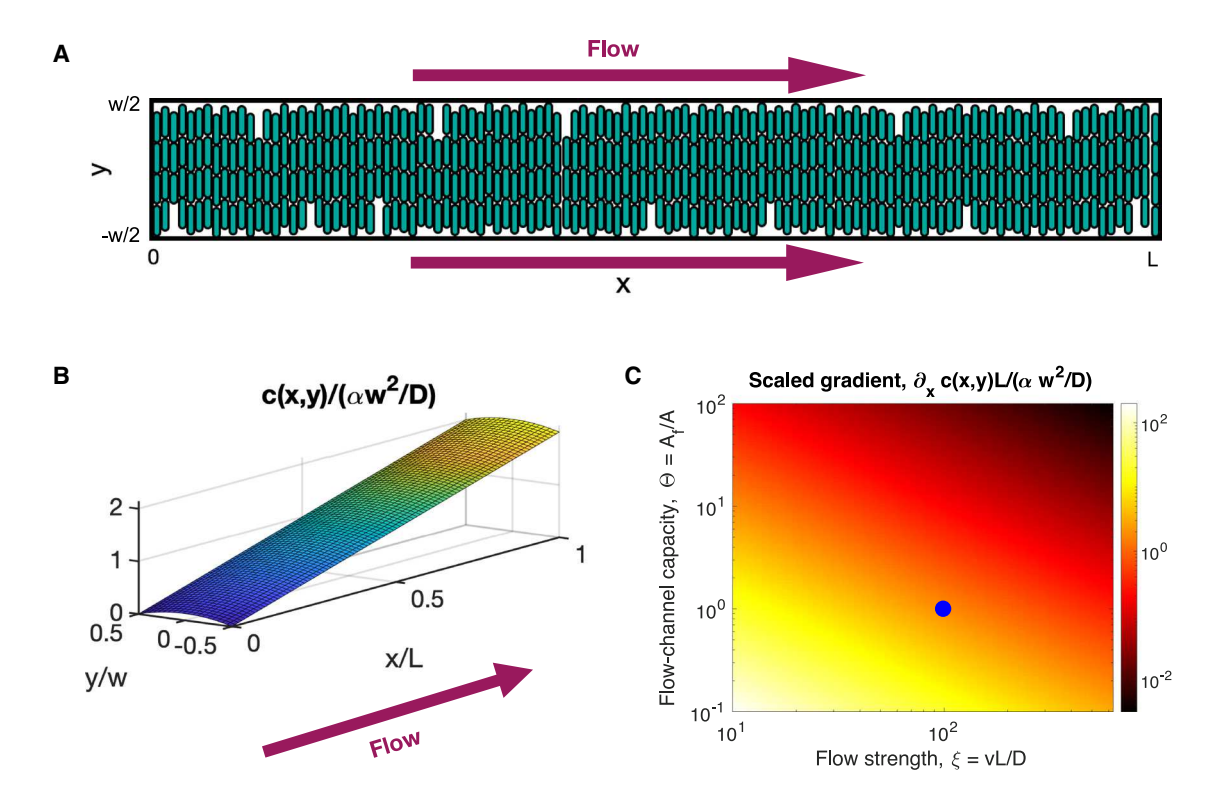


FIGURE 3 Effects of boundary flow. (A) Rightward flow is imposed at the upper and lower boundaries. (B) The flow induces a concentration gradient not just at the boundaries (long edge), but also within the cell population (surface). (C) The gradient as a function of flow strength  $\xi$  and flow-channel capacity  $\Theta$ . (B and C) Plots of Eq. 17. Parameters are  $\xi = 100$ ,  $\Theta = 1$ , and aspect ratio  $\varphi = L/w = 20$  in (B) and  $\varphi = 20$  in (C). The plot in (B) corresponds to the blue circle in (C). To see this figure in color, go online.

relative to other scales in the system. The mixing timescale in a cross section of a flow channel is given by  $A_f/D$ . The corresponding advective lengthscale in the flow channel is  $(A_f/D)v$ . Using typical experimental values (10)  $D = 500 \ \mu\text{m}^2/\text{s}$ ,  $A_f = 10 \ \mu\text{m} \times 10 \ \mu\text{m}$ , and v =25  $\mu$ m/s, the advective lengthscale becomes 5  $\mu$ m, a lengthscale that is a mere 1/400 fraction of the length of a 2 mm flow channel.

Because b no longer depends on y, the net flux of signal into the flow channels can no longer be accounted for by enforcing continuity of the y-derivative at the boundaries. Instead, this flux appears as an effective source term in Eq. 13, whose magnitude is determined by flux balance. Specifically, in a slice of length  $\Delta x$ , the flux of signaling molecules out of the trapping region,  $\alpha A \Delta x$ , must equal the flux into the two flow channels,  $\widehat{\alpha}(2A_f)\Delta x$ . Thus, the effective source term is  $\hat{\alpha} = \alpha/2\Theta$  for the area ratio  $\Theta = A_f/A$ , which we refer to as the flow-channel capacity. Correspondingly, Eq. 13 becomes

$$\dot{b} = D\partial_x^2 b - v\partial_x b + \alpha/2\Theta. \tag{15}$$

We solve Eq. 15 in steady state by direct integration in appendix B, where we show that, for long flow channels with sufficiently fast flow, the profile b(x) in the bulk is insensitive to the boundary conditions at x = 0 and x = L. In the bulk, the profile is linear in x,

$$b(x) = \frac{\alpha}{2\Theta v} x,\tag{16}$$

which satisfies Eq. 15 by inspection. The linearity of Eq. 16 validates the effective source term  $\alpha/2\Theta$  in Eq. 15. This term is a local approximation in x for the rate of increase of flow channel concentration due to diffusive coupling with the trapping region under a flux balance argument. The linearity enforces the flux balance approximation because the diffusion operator in Eq. 12 satisfies  $\nabla^2[c(x,y)+b(x)] = \nabla^2c(x,y)$  when b is linear. The resulting c(x, y) is quadratic in y, linear in x, and satisfies the boundary condition in Eq. 14,

$$c(x,y) = \frac{\alpha w^2}{D} f(y) + \frac{\alpha}{2\Theta v} x,$$
 (17)

where f(y) is given by Eq. 4.

Eqs. 16 and 17 are shown in Fig. 3 B: c(x, y) is the surface and b(x) is the long edge. We see that the concentration increases not only in the flow channels (the edge), but also within the cell population (the surface). Thus, diffusive coupling between the flow channels and the trapping region induces a signal gradient in the cell population, even though the population itself is not subjected to the flow.

To get a sense of the magnitude of the gradient within the cell population, we plot in Fig. 3 C the derivative  $\partial_x c(x, y)$ , scaled by the characteristic lengthscale w and concentration value  $\alpha w^2/D$ , as a function of the flow strength and the flowchannel capacity  $\Theta$ . For the flow strength, we use the Péclet number of the flow channel  $\xi = vL/D$  (a dimensionless determinant of the flow speed relative to diffusion), in terms of which the scaled derivative reads  $\varphi^2/2\Theta\xi$ , where  $\varphi=L/2\Theta\xi$ w is the aspect ratio of the trapping region. We see that the gradient vanishes for large  $\Theta$  and  $\xi$  but can be large otherwise. For example, the case plotted in Fig. 3 B, corresponding to the blue circle in Fig. 3 C, has parameters estimated from recent microfluidic experiments with E. coli (10), and we see that the gradient is substantial. Our results are valid for  $\xi$  large, to justify the bulk assumption (Appendix B), and  $\Theta$  not too large, to justify the assumption of a well-mixed flow channel as discussed above. We see in Fig. 3 C that the experimental parameters,  $\xi = 100$ and  $\Theta = 1$ , are consistent with these assumptions. We comment further on experimental comparisons in the discussion.

#### DISCUSSION

We described and analyzed a tractable model to explain how advective-diffusive boundary conditions shape signaling response in spatially extended microbial communities. We assumed bacteria are trapped in a monolayer within a region bounded by two adjacent channels through which fluid flows. With absorbing channels, we found that the signaling lengthscale is determined (or, with degradation, bounded) by the monolayer geometry, not the diffusion coefficient, because diffusion disperses molecules but also hastens their loss at the boundaries. We also found that flow at the boundaries can induce significant signal gradients in the population and that this effect is most pronounced with small flow channels at intermediate flow speeds. Although we based the model on a microfluidic trap setting, a similar approach can be used to describe more general situations. For instance, a thin bacterial film growing in a pipe could be modeled by assuming that an adjacent channel lies above a layer of cells.

Our results could have significant impact on QS in microbial populations. A principal function of QS circuits in natural systems is the detection of a quorum of cells that triggers induction of a gene network. For example, a QS signal can trigger the production of proteins that release the extracellular matrix so that cells move to a mobile state under starvation (2). Pai and You have described this as the QS circuit's sensing potential, which depends on the local environment and a threshold level of signaling molecule sensed by the cell (3). Our results can be used to generalize this sensing potential framework to include environmental influence on QS activation. We did not model cellular responses to the QS signal, but assumed that cells that express the signal do so uniformly. Bacteria can respond to QS signals in complex ways, however. Dalwadi and Pearce have

used a model similar to the one we analyzed to show that positive feedback can act as a low-pass filter and ensure a robust collective response to oscillatory flow (8). In their model the flow passes over the surface of a cell population trapped in a pocket. Their analytical results are based on the assumption that diffusion across this surface dominates the diffusion in the direction of the flow, allowing them to derive a tractable one-dimensional PDE for the signal concentration in the direction perpendicular to the flow.

Our model provides several experimentally testable predictions. First, for bacterial collectives growing in geometries with open boundaries, chemical signaling depth can be independent of the diffusion rate of the signaling molecule. Second, when a flow channel borders a bacterial collective, signaling molecule flux into the flow channel can induce a graded signal concentration profile there. This graded profile in the flow channel can induce signaling molecule concentration gradients within the bacterial collective, even when the bacterial collective is isogenic. In this way, flow may play a role in differentiation. These predictions are testable, as bacteria such as *E. coli* can be engineered to respond to the presence of a QS signal by producing a fluorescent protein in a graded manner, or when signal concentration reaches a threshold.

As a first step in comparing our results with experiments, we can consider a previous study in which a sender-receiver system of the type in Fig. 2 A was constructed in a microfluidic device (10). The height of the trapping region was  $w = 100 \mu m$ , from which Eq. 6 predicts that the signal should extend for a lengthscale of  $\Lambda \approx w/\pi \approx 32 \mu m$ . The measured lengthscale was  $\Lambda = 20 \,\mu\text{m}$ , which agrees within a factor of two. The prediction could be refined by considering the effects of boundary flow (Fig. 3) on the senderreceiver geometry (Fig. 2), which could conceivably increase the predicted lengthscale (the experimental parameters  $L = 2000 \, \mu \text{m}$ ,  $D = 500 \, \mu \text{m}^2/\text{s}$ ,  $v \sim 25 \, \mu \text{m/s}$ ,  $A = 100 \ \mu \text{m} \times 1 \ \mu \text{m}$ , and  $A_f = 10 \ \mu \text{m} \times 10 \ \mu \text{m}$  give  $\xi = vL/D = 100$ ,  $\Theta = A_f/A = 1$ , and  $\varphi = L/w =$ 20, as in Fig. 3 B). On the other hand, the fact that cells in the experiment are nematically ordered with their long axis pointing toward the open boundaries, as in Fig. 2 A (15,16), could conceivably decrease the predicted lengthscale because diffusing molecules are subject to steric barriers more often in the x-direction than in the y-direction. Even without these refinements, it is encouraging that our prediction is close to the experimental observation.

Our modeling could be extended, for example, to include diffusion of signaling molecules across the cell membranes (see, e.g., (3-5)). Currently, we assumed that cell-internal and cell-external signaling molecule concentrations are equal at steady state. This is tantamount to assuming that the diffusion rate of signaling molecules through the cell membrane, d, is infinite. When d is low, however, the cross-membrane timescale, which scales as  $d^{-1}$ , can become important. First, when  $0 < d < \infty$ , in steady state

cell-internal and cell-external signaling molecule concentrations will differ in the trapping domain. This difference will increase as d decreases. Second, when the cell membrane is impermeable (d = 0), cells will sequester all of the signaling molecules they produce before said cells exit the trapping region, resulting in no signaling through the extracellular space. This sequestration effect will continue to limit cell-cell signaling efficacy when d > 0, provided the  $d^{-1}$  timescale is long relative to other system timescales.

Importantly, our work suggests careful examination of mathematical models used for open-boundary signaling systems, for example, in microfluidics with advective fluid flow. If the chemical degradation timescales are long (25) relative to signaling-region residence times, then a model such as Eq. 1 should appear without a first-order degradation term. Steady-state signaling profiles then depend on appropriate inclusion of boundary conditions to account for signal loss, which may require more sophisticated mathematical techniques for the resulting solution, e.g., Eq. 5. We anticipate that further analysis of timescales for reaction-advection-diffusion systems and other modeling advances can be included in future work.

#### **APPENDIX A**

Here, we derive Eq. 9. As mentioned in the main text, Eq. 5 follows in the limit of no degradation ( $\lambda \gg w$ ).

In the receiver domain ( $x \ge 0$ ), the source term  $\alpha$  is absent from Eq. 7. Separating variables as c(x, y) = X(x)Y(y), Eq. 7 in steady state in this domain becomes

$$\frac{\partial_x^2 X}{X} + \frac{\partial_y^2 Y}{Y} = \frac{1}{\lambda^2},\tag{18}$$

where  $\lambda = \sqrt{D/\gamma}$ . Because the two terms on the left are each a function of a different variable, and both sum to a constant, they must each equal a constant themselves. Calling the second term's constant  $-q^2/w^2$  for some unknown q, we have  $\partial_y^2 Y/Y = -q^2/w^2$ , whose general solution is

$$Y(y) = B\sin(qy/w) + C\cos(qy/w). \tag{19}$$

The boundary conditions in Eq. 2 require that B = 0 and q = $\pi(2n+1) \equiv q_n$  for nonnegative integer n. The first term in Eq. 18 then satisfies  $\partial_x^2 X/X = q_n^2/w^2 + 1/\lambda^2 \equiv 1/\ell_n^2$ , whose general solution is

$$X(x) = Ee^{x/\ell_n} + Ge^{-x/\ell_n}.$$
 (20)

The boundary condition in Eq. 3 requires that E = 0. Thus, the solution in the receiver domain is

$$c(x \ge 0, y) = \frac{\alpha w^2}{D} \sum_{n=0}^{\infty} A_n e^{-x/\ell_n} \cos(q_n y / w)$$
 (21)

for some unknown  $A_n$ .

In the sender domain (x < 0), the source term  $\alpha$  is present in Eq. 7. We write the steady-state solution in this domain as the sum of a particular solution, which is any function that satisfies Eq. 7 with  $\alpha$  present, and the homogeneous solution, which satisfies Eq. 7 with  $\alpha$  absent. For the particular solution we use the limit far from the receiver cells, Eq. 8. For the homogeneous solution, we use Eqs. 19 and 20, where again B = 0, but in this domain G = 0 to prevent the solution from diverging as  $x \to -\infty$ . Thus,

$$c(x < 0, y) = \frac{\alpha w^2}{D} \left[ F(y) + \sum_{n=0}^{\infty} H_n e^{x/\ell_n} \cos(q_n y / w) \right]$$
(22)

for some unknown  $H_n$ , where F(y) is as in Eq. 8.

Differentiating Eqs. 21 and 22 with respect to x, we see that continuity of the derivative at x = 0 requires that  $H_n = -A_n$  for all n due to the orthogonality of the cosines. Continuity of the solution at x = 0 then requires

$$2\sum_{n=0}^{\infty} A_n \cos(q_n y / w) = F(y).$$
 (23)

The orthogonality of cosines, expressed as

$$\int_{-w/2}^{w/2} dy \cos(q_m y / w) \cos(q_n y / w) = \frac{w}{2} \delta_{mn}, \qquad (24)$$

allows us to invert Eq. 23,

$$A_n = \frac{1}{w} \int_{-w/2}^{w/2} dy \, F(y) \cos(q_n y / w). \tag{25}$$

Inserting F(y) from Eq. 8 and evaluating the integrals yields

$$A_n = \frac{2(-1)^n \ell_n^2}{a_n w^2}. (26)$$

This completes the derivation of Eq. 9.

#### APPENDIX B

Here, we show that, for long channels with sufficiently fast flow, the profile b(x) in the bulk is linear and insensitive to the boundary conditions. We will illustrate this point by using two different choices for the boundary condition at x = L and showing that the bulk profile is the same linear function of x for both choices.

The bulk is defined by values of x that are small compared with the size of the system in that direction, L, but large compared with the characteristic lengthscale of the system. The characteristic lengthscale is a function of diffusion and flow speed and consequently required by dimensional analysis to scale as D/v. Thus, the bulk is defined by  $D/v \ll x \ll L$ . Dividing by L and recalling that  $\xi = vL/D$ , this expression becomes

$$1/\xi \ll x/L \ll 1. \tag{27}$$

Defining  $\epsilon = x/L$ , the two conditions in Eq. 27 become

$$\xi \epsilon \gg 1,$$
 (28)

$$\epsilon \ll 1,$$
 (29)

respectively. For a bulk regime to exist, the two extremes in Eq. 27 must be well separated, and therefore we must also have  $1/\xi \ll 1$ , or

$$\xi \gg 1.$$
 (30)

Given that  $\xi = vL/D$ , Eq. 30 makes clear that a bulk regime exists for sufficiently long channels (large L) with sufficiently fast flow (large v).

Eq. 15 in steady state is solved by directly integrating to find  $\partial_x b$  and integrating again to find b(x). Enforcing the boundary conditions b(0) = b(L) = 0 to set the integration constants and writing the result in terms of  $\epsilon$  obtains

Winkle et al.

$$b(x) = \frac{\alpha L}{2\Theta v} \left( \epsilon - \frac{1 - e^{\xi \epsilon}}{1 - e^{\xi}} \right). \tag{31}$$

Eqs. 28 and 30 allow us to neglect the ones in the numerator and denominator, respectively, giving

$$b(x) = \frac{\alpha L}{2\Theta v} \left[ \epsilon - e^{\xi(\epsilon - 1)} \right]. \tag{32}$$

Eq. 29 allows us to neglect the  $\epsilon$  in the exponent, and Eq. 30 then allows us to neglect the exponential altogether, giving

$$b(x) = \frac{\alpha}{2\Theta v}x,\tag{33}$$

where we have restored  $\epsilon = x/L$ . We see that b(x) is a linear function of x in the bulk.

Alternatively, we may have the boundary conditions b(0) = 0 and  $\partial_x b_{x=L} = 0$ , which correspond to rapid flushing of signaling molecules with fresh medium at x = 0, and steady-state accumulation downstream for x > L. The solution of Eq. 15 that satisfies these conditions is

$$b(x) = \frac{\alpha L}{2\Theta v} \left( \epsilon + \frac{1 - e^{\xi \epsilon}}{\xi e^{\xi}} \right). \tag{34}$$

Again, Eq. 28 allows us to neglect the one in the numerator, giving

$$b(x) = \frac{\alpha L}{2\Theta v} \left[ \epsilon - \frac{e^{\xi(\epsilon - 1)}}{\xi} \right], \tag{35}$$

and Eq. 29 allows us to neglect the  $\epsilon$  in the exponent, at which point Eq. 30 allows us to neglect the exponential term altogether, giving

$$b(x) = \frac{\alpha}{2\Theta v} x,\tag{36}$$

where we have once again restored  $\epsilon = x/L$ . Eq. 36 is the same as Eq. 33, showing that the bulk profile is insensitive to the choice of boundary condition

#### **AUTHOR CONTRIBUTIONS**

J.J.W., M.R.B., W.O., K.J., and A.M. designed the research. J.J.W., S.S., and J.E. performed the research and contributed analytic tools. J.J.W., S.S., W.O., K.J., and A.M. wrote the manuscript.

#### **ACKNOWLEDGMENTS**

This work was supported by National Science Foundation grants DMS-1816315 (to W.O.), MCB-1936774 (to M.R.B.), MCB-1936770 (to K.J.), and MCB-1936761 (to A.M.), and by National Institutes of Health grant R01-GM144959 (to M.R.B. and K.J.). This work was completed in part with resources provided by the Research Computing Data Core at the University of Houston.

#### **DECLARATION OF INTERESTS**

The authors declare no competing interests.

#### **REFERENCES**

 Levin, M. 2021. Bioelectric signaling: reprogrammable circuits underlying embryogenesis, regeneration, and cancer. *Cell.* 184:1971–1989. https://doi.org/10.1016/j.cell.2021.02.034.

- Emerenini, B. O., B. A. Hense, ..., H. J. Eberl. 2015. A mathematical model of quorum sensing induced biofilm detachment. *PLoS One*. 10, e0132385. https://doi.org/10.1371/journal.pone.0132385.
- 3. Pai, A., and L. You. 2009. Optimal tuning of bacterial sensing potential. Mol. Syst. Biol. 5:286. https://doi.org/10.1038/msb.2009.43.
- Danino, T., O. Mondragón-Palomino, ..., J. Hasty. 2010. A synchronized quorum of genetic clocks. *Nature*. 463:326–330. https://doi. org/10.1038/nature08753.
- Chen, Y., J. K. Kim, ..., M. R. Bennett. 2015. Emergent genetic oscillations in a synthetic microbial consortium. *Science*. 349:986–989. https://doi.org/10.1126/science.aaa3794.
- Boo, A., R. Ledesma Amaro, and G.-B. Stan. 2021. Quorum sensing in synthetic biology: a review. *Curr. Opin. Struct. Biol.* 28, 100378. https://doi.org/10.1016/j.coisb.2021.100378.
- Wartlick, O., A. Kicheva, and M. González-Gaitán. 2009. Morphogen gradient formation. *Cold Spring Harb. Perspect. Biol.* 1:a001255. https://doi.org/10.1101/cshperspect.a001255.
- Dalwadi, M. P., and P. Pearce. 2021. Emergent robustness of bacterial quorum sensing in fluid flow. *Proc. Natl. Acad. Sci. USA*. 118, e2022312118. https://doi.org/10.1073/pnas.2022312118.
- Kirisits, M. J., J. J. Margolis, ..., M. R. Parsek. 2007. Influence of the hydrodynamic environment on quorum sensing in Pseudomonas aeruginosa biofilms. *J. Bacteriol*. volume 189:8357–8360. https://doi.org/ 10.1128/JB.01040-07.
- Alnahhas, R. N., J. J. Winkle, ..., M. R. Bennett. 2019. Spatiotemporal dynamics of synthetic microbial consortia in microfluidic devices. ACS Synth. Biol. 8:2051–2058. https://doi.org/10.1021/acssynbio.9b00146.
- Janakiraman, V., D. Englert, ..., H. Baskaran. 2009. Modeling growth and quorum sensing in biofilms grown in microfluidic chambers. *Ann. Biomed. Eng.* 37:1206–1216. https://doi.org/10.1007/s10439-009-9671-8.
- Dalwadi, M., and P. Pearce. 2021. Robustness and precision of bacterial quorum sensing in fluid flow. *Biophys. J.* 120:261a. https://doi.org/10. 1016/j.bpj.2020.11.1676.
- Winkle, J. J., B. R. Karamched, ..., K. Josić. 2021. Emergent spatiotemporal population dynamics with cell-length control of synthetic microbial consortia. *PLoS Comput. Biol.* 17, e1009381. https://doi.org/10. 1371/journal.pcbi.1009381.
- Kim, J. K., Y. Chen, ..., M. R. Bennett. 2019. Long-range temporal coordination of gene expression in synthetic microbial consortia. *Nat. Chem. Biol.* 15:1102–1109. https://doi.org/10.1038/s41589-019-0372-9.
- Karamched, B. R., W. Ott, ..., K. Josić. 2019. Moran model of spatial alignment in microbial colonies. *Physica D*. 395:1–6. https://doi.org/ 10.1016/j.physd.2019.02.001.
- Volfson, D., S. Cookson, ..., L. S. Tsimring. 2008. Biomechanical ordering of dense cell populations. *Proc. Natl. Acad. Sci. USA*. 105:15346–15351. https://doi.org/10.1073/pnas.0706805105.
- O'Toole, G. A., and R. Kolter. 1998. Flagellar and twitching motility are necessary for *Pseudomonas aeruginosa* biofilm development. *Mol. Microbiol.* 30:295–304. https://doi.org/10.1046/j.1365-2958. 1998.01062.x.
- Seminara, A., T. E. Angelini, ..., M. P. Brenner. 2012. Osmotic spreading of *Bacillus subtilis* biofilms driven by an extracellular matrix. *Proc. Natl. Acad. Sci. USA*. 109:1116–1121. https://doi.org/10. 1073/pnas.1109261108.
- Gloag, E. S., L. Turnbull, ..., C. B. Whitchurch. 2013. Self-organization of bacterial biofilms is facilitated by extracellular DNA. *Proc. Natl. Acad. Sci. USA*. 110:11541–11546. https://doi.org/10.1073/pnas.1218898110.
- Abisado, R. G., S. Benomar, ..., J. R. Chandler. 2018. Bacterial quorum sensing and microbial community interactions. *mBio*. 9, e02331-17. https://doi.org/10.1128/mbio.02331-17.
- Mukherjee, S., and B. L. Bassler. 2019. Bacterial quorum sensing in complex and dynamically changing environments. *Nat. Rev. Microbiol*. 17:371–382. https://doi.org/10.1038/s41579-019-0186-5.

- 22. Zong, D. M., M. Sadeghpour, ..., M. R. Bennett. 2022. Tunable dynamics in a multi-strain transcriptional pulse generator. Preprint at bio-Rxiv. https://doi.org/10.1101/2022.09.23.509237.
- 23. Deter, H. S., and T. Lu. 2022. Engineering microbial consortia with rationally designed cellular interactions. Curr. Opin. Biotechnol. 76, 102730. https://doi.org/10.1016/j.copbio.2022.102730.
- 24. Alnahhas, R. N., M. Sadeghpour, ..., M. R. Bennett. 2020. Majority sensing in synthetic microbial consortia. Nat. Commun. 11:3659. https://doi.org/10.1038/s41467-020-17475-z.
- 25. Trovato, A., F. Seno, ..., A. Squartini. 2014. Quorum vs. diffusion sensing: a quantitative analysis of the relevance of absorbing or reflecting boundaries. FEMS Microbiol. Lett. 352:198-203. https://doi.org/ 10.1111/1574-6968.12394.
- 26. Carslaw, H., and J. Jaeger. 1959. Conduction of Heat in Solids. Clarendon Press.
- 27. Crank, J. 1979. The Mathematics of Diffusion. Oxford university press.
- 28. Dong, Y.-H., J.-L. Xu, ..., L.-H. Zhang. 2000. AiiA, an enzyme that inactivates the acylhomoserine lactone quorum-sensing signal and atten-

- uates the virulence of Erwinia carotovora. Proc. Natl. Acad. Sci. USA. 97:3526-3531. https://doi.org/10.1073/pnas.97.7.3526.
- 29. Cao, Y., S. He, ..., B. Yao. 2012. Orally administered thermostable N-Acyl homoserine lactonase from Bacillus sp. strain AI96 attenuates aeromonas hydrophila infection in zebrafish. Appl. Environ. Microbiol. 78:1899-1908. https://doi.org/10.1128/aem.06139-11.
- 30. Ferry, M., I. Razinkov, and J. Hasty. 2011. Microfluidics for synthetic biology. In Methods in Enzymology Elsevier, pp. 295-372. https://doi. org/10.1016/b978-0-12-385075-1.00014-7.
- 31. Gulati, S., V. Rouilly, ..., A. J. deMello. 2009. Opportunities for microfluidic technologies in synthetic biology. J. R. Soc. Interface. 6:S493-S506. https://doi.org/10.1098/rsif.2009.0083.focus.
- 32. Kachiashvili, K., D. Gordeziani, ..., D. Melikdzhanian. 2007. Modeling and simulation of pollutants transport in rivers. Appl. Math. Model. 31:1371-1396. https://doi.org/10.1016/j.apm.2006. 02.015.
- 33. Bresch, D. 2009. Shallow-water equations and related topics. In Handbook of Differential Equations - Evolutionary Equations Elsevier, pp. 1-104. https://doi.org/10.1016/s1874-5717%2808%2900208-9.